2D Materials

PAPER

Structural and electronic properties of two-dimensional titanium carbo-oxides

To cite this article: Yong-Jie Hu *et al* 2023 *2D Mater.* **10** 015019

View the article online for updates and enhancements.

You may also like

- Substitutional carbon doping of free-standing and Ru-supported BN sheets: a first-principles study
N Berseneva, H-P Komsa, V Vierimaa et al.
- Substitutional C on B sites in $AlLiB_{14}$
L F Wan and S P Beckman
- Development of high performance $Pr_2(Fe, Co)_{14}B$/-(Fe, Co)-type nanocomposite ribbons by Co/Ti/C substitution
C H Chiu, C H Chen, C W Chang et al.

This content was downloaded from IP address 144.118.76.222 on 23/06/2023 at 22:03

2D Materials

RECEIVED
14 September 2022

REVISED
24 November 2022

ACCEPTED FOR PUBLICATION
4 December 2022

PUBLISHED
20 December 2022

PAPER

Structural and electronic properties of two-dimensional titanium carbo-oxides

Yong-Jie Hu[1,*], Christopher Tandoc[1], Michel W Barsoum[1,2], Johanna Rosen[2] and Jonas Björk[2,*]

[1] Department of Material Science and Engineering, Drexel University, Philadelphia, PA, United States of America
[2] Materials Design Division, Department of Physics, Chemistry and Biology (IFM), Linköping University, Linköping, Sweden
[*] Authors to whom any correspondence should be addressed.

E-mail: yh593@drexel.edu and jonas.bjork@liu.se

Keywords: first-principles calculations, electronic structures, crystal structure prediction, titanium oxides

Supplementary material for this article is available online

Abstract

This work was inspired by new experimental findings where we discovered a two-dimensional (2D) material comprised of titanium-oxide-based one-dimensional (1D) sub-nanometer filaments. Preliminary results suggest that the 2D material contains considerable amounts of carbon, C, in addition to titanium, Ti, and oxygen, O. The aim of this study is to investigate the low-energy, stable atomic forms of 2D titanium carbo-oxides as a function of C content. Via a combination of first-principles calculations and an effective structure sampling scheme, the stable configurations of C-substitutions are comprehensively searched by templating different 2D TiO_2 polymorphs and considering a two O to one C replacement scheme. Among the searched stable configurations, a structure where the (101) planes of anatase bound the top and bottom surfaces with a chemical formula of $TiC_{1/4}O_{3/2}$ was of particularly low energy. Furthermore, the variations in the electronic band structure and chemical bonding environments caused by the high-content C substitution are investigated via additional calculations using a hybrid exchange-correlation functional.

1. Introduction

Twenty years ago, the discovery of graphene opened the door to a new compositional and structural space of two-dimensional (2D) materials [1]. Since then, 2D materials such as *h*BN [2], silicene [3], germanene [4], 2D transition metal oxides [5] dichalcogenides [6], and Mxenes [7], have been extensively explored because of their unique combination of functional properties that is different from the respective three-dimensional (3D) bulk counterpart. One currently generic approach for 2D materials synthesis is to exfoliate 2D sheets from their 3D bulk precursors, which are generally layered solid crystals like graphite, transition metal dichalcogenides, layered oxides, and more recently, the MAX phases [8–11]. Another approach is to synthesize 2D materials using a bottom-up approach. The latter include chemical vapor deposition [12], on-surface reactions both at the solid-liquid interface [13] and under ultrahigh vacuum conditions [14, 15], and soft chemistry approaches [16, 17]. Among these bottom-up approaches, soft chemistry such as sol-gel synthesis has shown great promise for the scalable production with high morphological, chemical, and structural control of the final 2D products.

The synthesis of 2D titania (TiO_2) is among the successful examples of the soft chemistry approach. In the past, TiO_2 has been more extensively studied in its 3D bulk phases, such as anatase and rutile, due to its superior functionalities promising for a variety range of applications from photocatalysis [18] and photovoltaics [19] to lithium, Li, and beyond Li batteries [20, 21]. More recently, the 2D TiO_2 nanosheets with atomic-level thicknesses has attracted a great deal of attention as they possess not only the common merits of nanomaterials, such as high surface area, high chemical activity, and intimate binding with other component materials, but also some outstanding electronic, optical, photochemical, and electrochemical properties uniquely arising from the confined atomic-level thickness [22–26]. Up to date, two types of 2D TiO_2 nanosheets have been synthesized as single-crystal nanoflakes with atomic-level thicknesses through a soft chemistry process [22, 23, 25, 27]. One possesses a crystal structure

© 2022 IOP Publishing Ltd

close to that of lepidocrocite which is a layered polymorphic structure of bulk TiO_2 [23, 27]. Besides, 2D TiO_2 has also been fabricated as atomic-thin nanoflakes with the non-equilibrium surfaces close to the anatase (010) and rutile (001) facets [25]. Both of these 2D structures show enlarged optical band gaps compared to their 3D bulk counterpart and are thus considered to be promising for applications in photovoltaic devices with higher open-circuit voltage [28]. Additionally, the higher conduction band edge of the 2D TiO_2 is also beneficial for H_2 production [23]. In addition to photovoltaic applications, the 2D TiO_2 with the lepidocrocite structure is also found to exhibit superior performance as a photoanode for dye-sensitized solar cells relative to the commercial Evonik's P25 TiO_2 [25, 29]. The ultrathin TiO_2 nanosheet can also serve as a 2D platform for loading other low-dimensional nanostructures such as semiconductor quantum dots and MXene to achieve unique combinations of functionalities that are hard to realize with single-type materials [26, 30].

Despite the variety of promising properties of 2D TiO_2, its synthesis to date still involves multistep complex solvent reactions and self-assembly oligomeric processes, which have led to issues such as the low crystallinity of the products. As such, cost-ineffective treatments at higher temperatures, such as calcination or hydrothermal synthesis, is generally required as a follow-up processes [31]. Quite recently we discovered a simple, one pot, near ambient almost universal process to convert carbides, nitrides, borides, silicides and, most crucially from an economic perspective, oxides into a plethora of nanomaterials, from one-dimensional (1D) nanofilaments, to 2D flakes, to quantum dots [32, 33]. The common factor in all our discoveries is the use of quaternary ammonium compounds, or quats, as near universal solvents as well as templating agents. Our process is scalable and results in high value-added materials quite inexpensively [32, 33].

More germane to this paper, we discovered that when powders of more than a *dozen* Ti-containing precursors such as TiC, TiB_2, TiN, MAX phases, silicides, etc are immersed in a 25 wt% tetramethylammonium hydroxide (TMAH) aqueous solution at 50 °C or 80 °C for a few days, they are transformed into anatase-based, C-containing, 1D nanofilaments, nfs, $\approx 6 \times 8$ Å^2 in cross-section. Henceforth, we are labeling these 1D materials, 1DA. Depending on post-reaction processing the 1DA self-assemble into highly ordered 2D flakes. The process is not restricted to TMAH, but also other quaternary ammonium compounds, or quats, such as TBAOH, TPAOH, etc. The quat's role is thus two-fold: almost universal solvent and templating agent [32].

More interestingly, the 1DA has been shown–be energy loss electron spectroscopy in a HRTEM, to contain high contents of carbon, C, in addition to Ti and O. In some locations that Ti:C:O atomic ratio was 1:1:1 [33]. The presence of a significant C content is new and departs from previously reported 2D TiO_2 structures. The introduction of C atoms into a TiO_2 2D lattice can be particularly useful in photocatalytic applications because the C atoms can lead to bandgap modifications which can improve the ability of the material to absorb visible light [34, 35]. However, C-containing TiO_2 has previously only been achieved in 3D bulk phases. As far as we are aware, our work is the first time substantial amounts of C were realized in low dimensional nanostructures. Therefore, despite the extensive experimental and computational studies on pristine TiO_2 [17, 24, 36, 37], the effects of C inclusions on the structural and physical properties of TiO_2-based 2D materials (henceforth referred to as 2D-TCO) remain overlooked.

There are several fundamental questions that have to be answered for 2D-TCO materials. For instance: does the 2D-TCO still possess the base crystal structure of C-free 2D TiO_2? If yes, what are the C substitution mechanisms, such as how many O atoms need to be replaced for each added C and which position does the C atom prefer to occupy? What are the effects of C substitution on the electronic band structure, such as a similar bandgap modification effect seen in the C-doped 3D TiO_2 [34, 35]? Before proceeding much further, it is important to note that our 2D flakes are quasi 2D in that they are comprised of 1DA nfs. This work is a first step towards understanding the latter. This comment notwithstanding, the work presented here is valid on its own, and strongly suggest that at least some of the 2D-TCO structures we modeled are experimentally possible.

To address these fundamental questions, herein, we carried out first-principles calculations based on density functional theory (DFT) to investigate the fundamental structural and electronic properties of the 2D-TCO sheets. Through a combination of DFT calculations and an atomic configuration sampling scheme, we effectively sampled the energy of multiple possible C-substitution configurations in several 2D TiO_2 template structures as a function of C concentration. Based on our screening results, a *low-energy, dynamically stable* 2D structure was identified. Based on the obtained atomic structure, further DFT calculations were performed to investigate the effects of C substitution on the electronic band structure, chemical bonding, as well as the elastic properties. This work enhances our fundamental understanding of 2D titanium carbo-oxide nanomaterials and makes predictions as to which are stable.

2. Method

The Vienna *ab-initio* Simulation Package was employed to perform the first-principles calculations [38], using the projector-augmented wave method

[39]. For the structural optimization calculations we used a plane wave basis with a kinetic cutoff energy of 400 eV and the exchange-correlation effects treated according to the generalized gradient approximation using the Perdew, Burke, and Ernzerhof functional [40]. Brillouin zone integration was performed using the Gaussian smearing method, with a smearing width of 0.10 eV and a k-point density of 0.1 $Å^{-1}$ along the two directions in the 1st surface Brillouin zone. A slab model with periodicity along x and y directions was used to construct the simulation supercells, in which a vacuum region of 15 Å was added along the z-direction to eliminate the interactions between the 2D sheet with its periodic images. Structural optimization of all structures was done by optimizing the internal coordinates of the atoms until the residual forces were smaller than 0.01 eV $Å^{-1}$. Furthermore, for each structure the lengths of the two surface unit cell axes were optimized using the Broyden–Fletcher–Goldfarb–Shanno (BFGS) algorithm, as implemented in the SciPy python library, with gradients of the unit cell vector lengths calculated by finite differences. How the search of low-energy configurations with C substitution in different 2D TCOs polymorphs was performed is described in the main text.

Phonon spectra were calculated using the finite difference method as implemented in the Phonopy code. In order to impose rotational and translational invariances, force constants were corrected according to the Born–Huang condition and Huang invariances [41] using the hiPhive python package [42]. The electronic band structure and charge density of the screened low energy structures were calculated using the HSE06 hybrid exchange-correlation functional [43] with an increased kinetic cutoff energy of 600 eV. The contour plots of the differential charge density were generated using VESTA [44].

3. Results and discussion

Whether characterized experimentally or predicted computationally, multiple polymorphic 2D TiO_2 structures, including lepidocrocite, referred to as Lepi from this point forward [34], the 1 T phase [36], the 2D hexagonal nanosheets [37], and the 2D facets of the (010) and (101) planes of bulk *anatase* (hereafter referred to as 2DA-010 and 2DA-101), respectively [24] have been proposed and explored. To define a basis for our atomic structure search for TCOs, we first performed DFT relaxation calculations on all aforementioned polymorphic structures. The Lepi structure was found to have the lowest ground state energy and be dynamically stable. Additionally, we found that the pristine, C-free 2DA-101 and 2DA-010 structures were dynamically unstable, although they yield x-ray diffraction (XRD) spectra aligning well with the experimental observation [33]. This implies a crucial effect of the inclusion of C on the structural stability of 2D-TCO. Therefore, moving forward we only considered them as the starting basis to perform a search of the most stable structures of the general chemical formula,

$$TiC_{\Delta n_C}O_{2-\Delta n_O}, \quad (1)$$

where Δn_O is the amount of O removed and Δn_C is the amount of C added per formula unit. To do so, we considered the two scenarios $\Delta n_C = \Delta n_O$ and $\Delta n_C = \Delta n_O/2$. Figure 1 depicts the crystal structures of the three 2D-TiO_2 employed as starting materials. Both the respective primitive unit cells (green areas in top row in figure 1) and the geometries of the supercells used in the calculations are indicated by the solid rectangle. Notably, the 2DA-010 structure in the pure TiO_2 composition is only obtained by constraining the relative in-plane positions of the Ti atoms, otherwise it transforms into the Lepi structure.

In investigating the different C content, structures were generated by selecting O atoms in the supercell using a random number generator, considering 15–30 randomly generated structures for each composition. For, all the selected O atoms were replaced by C atoms, while for $\Delta n_C = \Delta n_O/2$, one of the two selected O atoms were replaced by C and the other was removed from the structures. We also added ordered structures manually as these were not likely to be represented among the randomly generated ones. In both scenarios, we removed different O amounts from the structure, between $\Delta n_O = 1/8$ and $\Delta n_O = 1$. Each generated structure was structurally optimized, including both the internal coordinates and the two in-plane unit cell axes (as described in the section 2). The most stable structures—when starting from each of the base structures—for different Δn_C and Δn_O, are summarized in figures S1–S6 in supplemental information, SI.

In figure 2 the results are shown for the scenario where two O atoms are replaced by one C ($\Delta n_C = \Delta n_O/2$). For each composition in the plot, the energy difference is given with respect to the most stable structure for that composition. Firstly, for pure 2D-TiO_2 the Lepi structure is the most stable one. For, the structures with C atoms sitting in the middle—rather than on the outside—of the Ti layers are the most stable. However, the type of structure being the most stable one depends on the C:O ratio. If a small amount of O is substituted ($\Delta n_O = 1/8$) a structure reminiscent of the Lepi structure is favored (figure 2(b)). Here O in the central layer is replaced by a C, and an additional O atom is removed from one of the two surfaces. And while it appears that the 2DA-010 structures are close in energy to the Lepi ones for this stoichiometry, it should be noted that *all* of them relax into a structure that is close to Lepi. This is in accordance with the behavior of the pure 2D-TiO_2 for which the 2DA-010 optimized into Lepi if not constrained

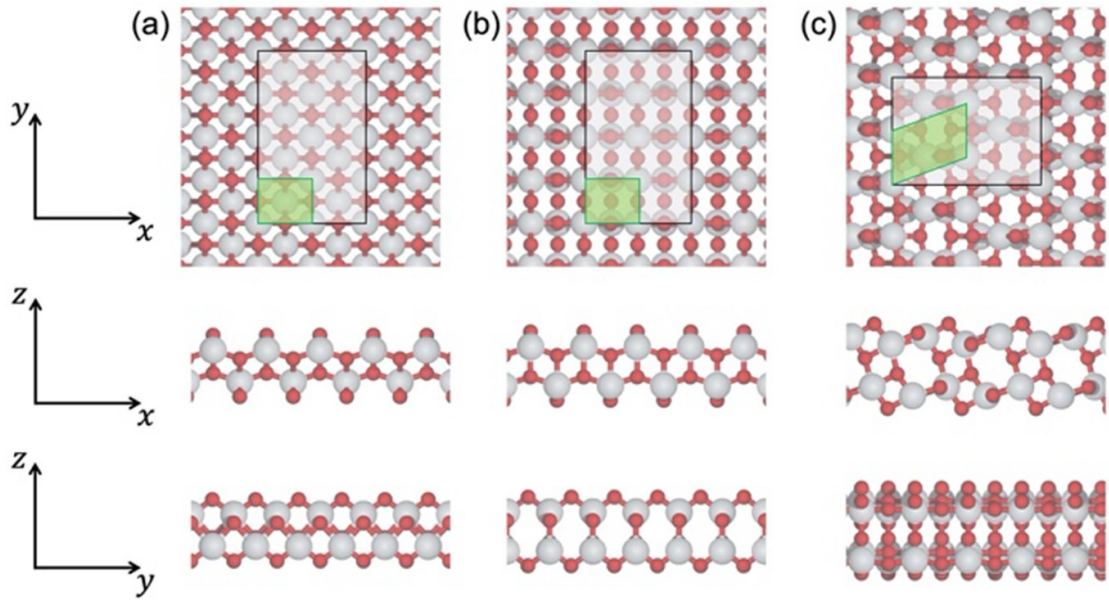

Figure 1. Structures of the 2D forms of TiO_2 considered as starting points in this study: (a) Lepi, (b) 2DA-010, and (c) 2DA-101. For each structure, the top view and two side views are shown, the directions of which are indicated by the Cartesian coordinate axes, where the *xy*-plane is in the propagation direction of the 2D structures and the *z*-axis is perpendicular to the 2D structures, i.e. the stacking direction. In the top view of each structure (top row), the primitive unit cell is indicated by the green area and the supercell used in the calculations is shown by the black frame.

(*vide supra*). Significantly, the 2DA-101 type structures stay in this geometry upon structural optimization and are closer to the Lepi in energy than for pure 2D-TiO_2.

Substituting a slightly higher O content ($\Delta n_O = 1/4$), the hierarchy between Lepi and 2DA-101 changes, such that a 2DA-101 type structure is the most stable one. This trend, going from Lepi to 2DA-101 upon reducing the O and increasing the C content, becomes most prominent for $\Delta n_O = 1/2$, for which we find a highly ordered structure significantly more stable than any other 2D material with the same composition. In this structure, the most centrally positioned O in the 2DA-101 are replaced in a way such that one C atom substitutes for two removed O atoms. The resulting structure closely resembles that of 2DA-101, but with the two bottom and two top Ti layers shifted with respect to each other. It is also possible to construct a primitive unit cell comparable to that of 2DA-101 (but with different lattice parameters). Notably, the simulated phonon spectrum of this structure shows that it is dynamically stable (figure S7).

Increasing the C content further, structures based on 2DA-101 become significantly distorted (cf figure S3 of SI for the most stable structure based on 2DA-101 for) as the C atoms need to be placed in the Ti layers, which is unfavorable. The most stable structure for $\Delta n_O = 1$ is based on Lepi that relaxes into a material with local resemblance of—and the same composition as—an O-terminated Ti_2C MXene (figure 2(e)) [45].

Now consider the scenario for which each O atom is replaced by a C atom in the 2D-TiO_2 structures, i.e. $\Delta n_C = \Delta n_O$. The results are summarized in figure 3. Like the scenario with $\Delta n_C = \Delta n_O/2$, the general trend is that the C atoms prefer to be in-between the Ti layers. However, for the most stable structures two adjacent O atoms are replaced by two C atoms such that the C atoms sit in dimers stabilized by a covalent bond. The trend when decreasing the amount of O is similar up to $\Delta n_O = 1/2$; a Lepi type structure is most stable for $\Delta n_O = 1/8$ (originating from a 2DA-010 initial structure), while the 2DA-101 type structures are most stable for $\Delta n_O = 1/4$ and. The structures for $\Delta n_O = 1$ have an equimolar mixture of Ti, C and O, and a structure based on 2DA-010 is found to be the most stable one (figure 3(e)). Notably, this structure has a quite close resemblance to 2DA-010 with the difference that one of the two Ti layers is translated in what is denoted as the *x*-direction in figure 2. This structure is considerably more stable than any other 2D material we investigated for this composition and found to be dynamically stable (figure S8). In this structure, the C dimers interlink the Ti atoms in one in-plane direction and the O atoms direct the growth in the perpendicular in-plane direction.

It is found that the stable structure corresponding to the formula of $TiC_{1/4}O_{3/2}$ (figure 2(d)), which is referred to as the 2DA-TCO structure from this point forward, yield a XRD pattern close to the experimental observations in our previous work of 1DA nanofilaments and their self-assembled 2D flakes [33]. Therefore, the electronic and elastic properties

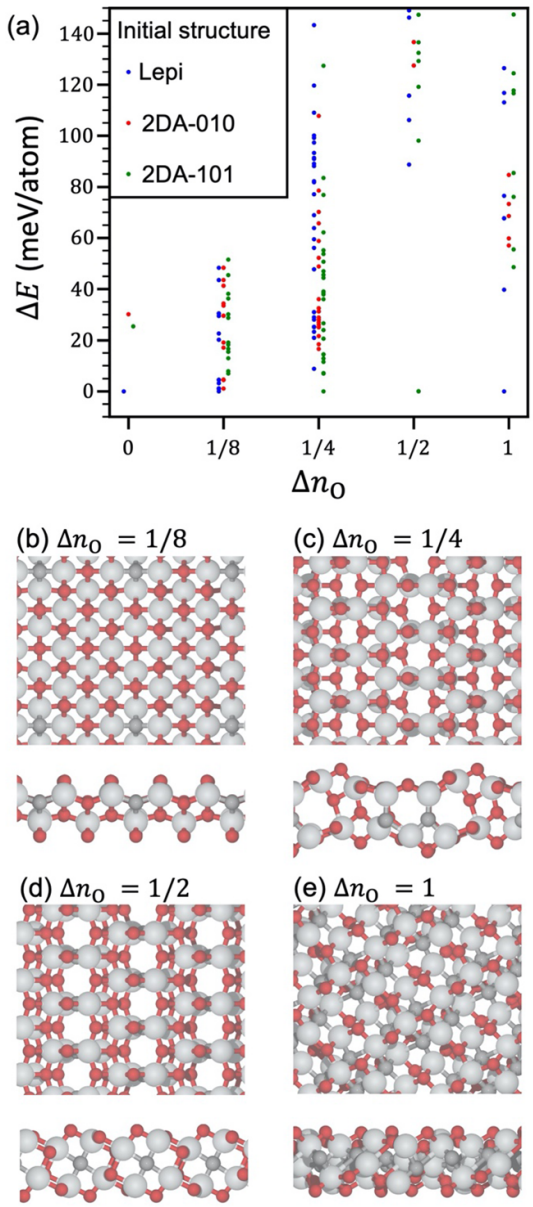

Figure 2. Results from a screening study of 2D TCOs, by replacing two O by one C atom from 2D-TiO_2 structures resulting in materials with the formula $TiC_{\Delta n_O/2}O_{2-\Delta n_O}$ (i.e. with $\Delta n_C = \Delta n_O/2$ in equation (1)), where the value of Δn_O is the amount of O replaced by C, or removed, from 2D-TiO_2. (a) Relative energies of the structures for each composition (indicated by Δn_O value) given with respect to the most stable structure for each composition. Each dot represents the energy of a material, and the color indicates which phase of 2D-TiO_2 it is based on prior to structural optimization but does not necessarily reflect the final optimized structure. (b)–(e) Top and side views of the most stable structures for the different compositions, as indicated.

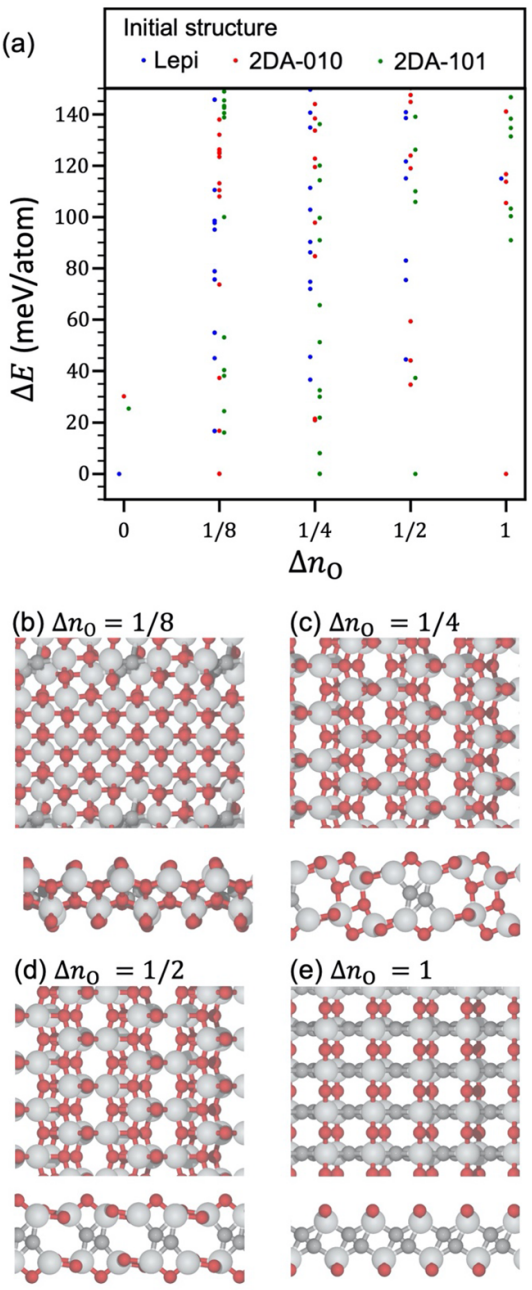

Figure 3. Results from a screening study of 2D TCOs, by replacing one O by one C from 2D-TiO_2 structures resulting in materials on the formula $TiC_{\Delta n_O}O_{2-\Delta n_O}$ (i.e. with $\Delta n_C = \Delta n_O$ in equation (1)), where the value of Δn_O describes amount of O replaced by C from 2D-TiO_2. (a) Relative energies of structures for each composition (indicated by Δn_O value) given with respect to most stable structure for each composition. Each dot represents the energy of a material, and the color indicates which phase of 2D-TiO_2 it is based on prior to structural optimization but does not necessarily reflect the final optimized structure. (b)–(e) Top and side views of the most stable structures for the different compositions, as indicated.

of the 2DA-TCO structure is further investigated using DFT calculations to provide some preliminary results/predictions for future studies and applications. The calculations of electronic structures were performed using a hybrid exchange-correlation functional, HSE06 [43], by which a more accurate description of the band gap and orbital hybridization can be expected.

The total and projected electronic density of states (DOSs) for the 2DA-101 and 2DA-TCO structures are shown in figures 4(a) and (b), respectively. As discussed above, 2DA-101 is the parent C-free structure of 2DA-TCO. In other words, the 2DA-TCO structure can be considered as a result of substituting every two central O atoms with one C atom in the 2DA-101

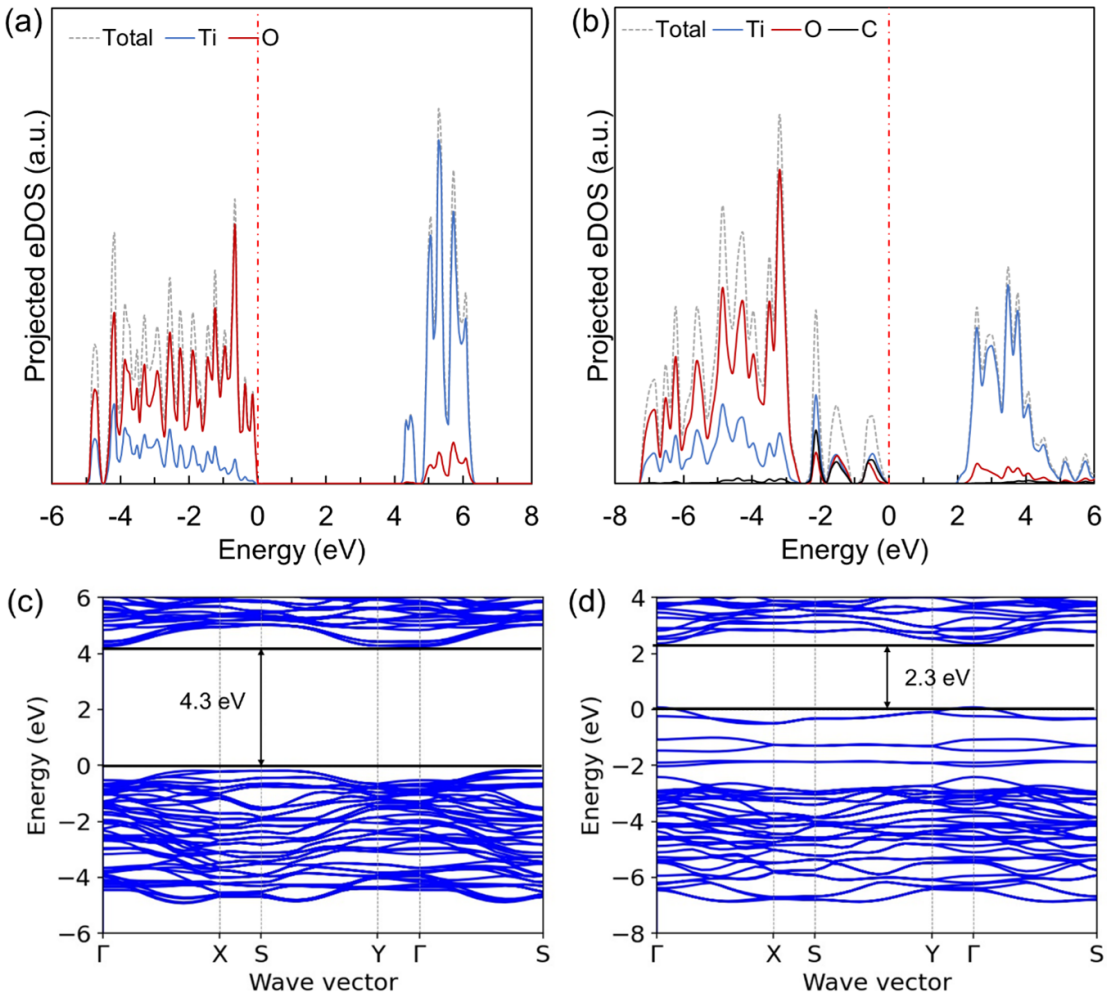

Figure 4. Total and projected electron density of states (DOSs) of, (a) the 2DA-101 and (b) 2DA-TCO structures. Electron band dispersion of (c) the 2DA-101 and (d) 2DA-TCO structures. Energy axes are rescaled to shift the upper edge of the valence band to be zero (i.e. all states below zero are occupied at 0 K).

structure. The band energy axes of the plots in figure 4 have been shifted such that the upper edge of the valence band is at zero (i.e. only states below zero are occupied). As shown in figure 4(a), the 2DA-101 structure has a relatively wide bandgap of about 4.3 eV, higher than that of the bulk anatase (3.2 eV experimentally and 3.6 eV computationally)[46]. A comparison between figures 4(a) and (b) suggests that the effects of C-atom substitutions on the electronic structure is relatively localized by adding a few new electronic states in the bandgap range of the pristine TiO_2 (i.e. 2DA-101). As shown in figure 4(b), those new states mainly correspond to a large overlap between the projected DOSs of Ti, C, and O, indicating that covalent bonds may form between the C and Ti atoms and the nearby O atoms. A further analysis indicates that the DOS overlap is mainly attributed to hybridizations between the *p* orbitals of the C and O atoms and the d_{yz}, d_{z2} and d_{x2-y2} orbitals of the Ti atoms. Similar C effects on the band structure have also been observed in the case of C-anion-doped 3D anatase TiO_2 [35].

To further scrutinize the C effects, the electronic band dispersions along high-symmetry directions in the first Brillouin zone for the 2DA-101 and 2DA-TCO structures are plotted in figures 4(c) and (d), respectively. Consistent with the DOS results, it is found that the C substitution does not significantly alter the valence or conduction bands structures but only introduces a few new states. These states are filled at 0 K, which shifts the valence band edge up by about 2.0 eV relative to 2DA-101, narrowing the bandgap to 2.3 eV. It is also worth noting that the existence of inter bandgap states is also revealed in the experimentally synthesized TCO nanoflakes via the UV–vis optical absorption spectra measurements [33].

To reveal the bonding features between the C atoms and their surrounding O and Ti atoms, we plot the differential charge densities ($\Delta\rho$) in figure 5. Here $\Delta\rho$ is defined as the difference between the charge densities from the self-consistent calculations and a non-self-consistent superposition of atomic charge densities of unbonded states. Therefore, the value of $\Delta\rho$ quantifies the charge transfer and redistribution

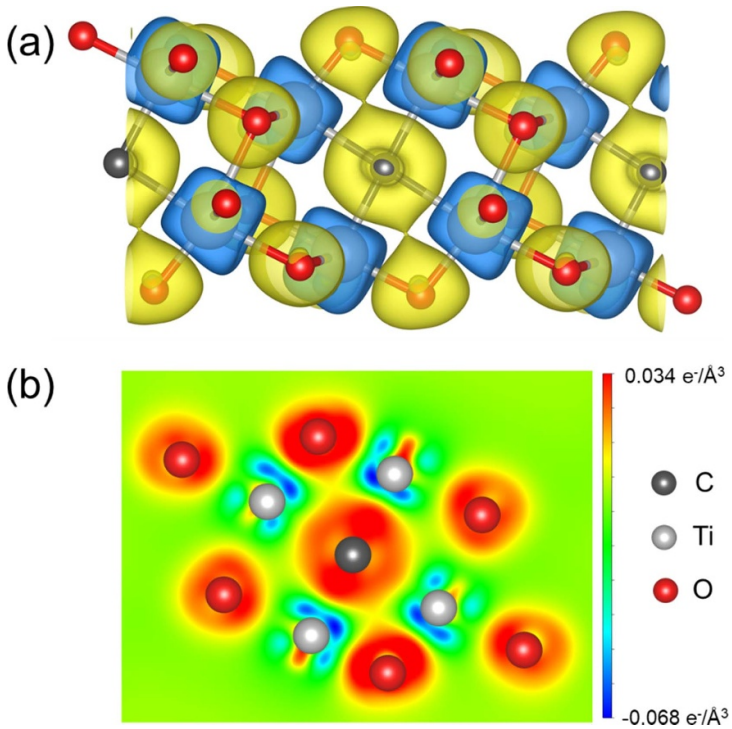

Figure 5. Differential charge density ($\Delta\rho$) of the 2DA-TCO structure. (a) 3D isosurface at $\Delta\rho = \pm 0.009\, e^-/\text{Å}$. (b) 2D contour plot of the plane on which the C atom lie together with its nearby Ti and O atoms.

due to the formation of chemical bonds between atoms [47, 48]. The 3D $\Delta\rho$ isosurface of 2DA-TCO is shown in figure 5(a) along with the atomic structure at $\Delta\rho = \pm 0.009\, e^-/\text{Å}$. Positive $\Delta\rho$ is rendered in yellow while the negative ones in blue. As shown in figure 5(a), considerable charge transfer from the Ti atoms to the C and O atoms is observed. To characterize the bonding features between those atoms in more detail, figure 5(b) shows a 2D contour plot of $\Delta\rho$ of the plane on which the C atoms lie together with their nearby Ti and O atoms. As shown in figure 5(b), after charge transfer, the valence electrons mainly accumulate around the O and C atoms with a spherical-like spatial distribution, implying an ionic characteristic of the Ti–C and Ti–O bonds. A Bader charge analysis was carried out to quantitatively estimate the charge transfer among the Ti, O, and C atoms. It was found that on average about 2.2 electrons transferred from each Ti atom to the adjacent O and C atoms. Each O atom averagely gained 1.2 electrons, while the average gain of the C atoms is about 1.6 electrons. This substantial charge transfer among the Ti, O, and C atoms confirms the strong ionic characteristic of the Ti–C and Ti–O atomic bonds. On the other hand, a denser accumulation of valence electrons can be found in the interatomic regions between C and Ti, implying the Ti–C bonds could also exhibit covalent characteristics, which is consistent with the orbital hybridization observed in figure 4(a). Additionally, a weak charge accumulation between C and O can be observed in figure 5(a), suggesting that in addition to the Ti–C and Ti–O bonds, a weak covalent bond may also exist between the C and O atoms, which accounts for the overlap between the project DOS curves of C and O shown in figure 4(a).

The elastic constants, c_{ij}s, of the 2DA-101 and 2DA-TCO structures were obtained by DFT calculations. The results are listed in table 1. It is found that the c_{ij}s of both structures satisfy the 'Born stability criteria' [49], indicating they are all mechanically stable. Except for c_{66}, the 2DA-TCO structure has higher elastic constants than the 2DA-101 structure, which is attributable to the formation of strong Ti–C bonds.

The practical synthesis of the 2DA-TCO structure discovered here could be non-trivial and warrant further studies in the future. The bottom-up synthesis strategy is considered to be more appropriate than the conventional top-down approaches for 2D materials synthesis because 3D polymorphic structures for titanium oxides are typically nonlayered. Previous attempts of synthesizing C-containing titanium oxides have mainly been focused on 3D bulk phases [34, 50–54], employing bottom-up like synthesis approaches, such as chemical vapor deposition [50], sol-gel reactions [34, 51], magnetron sputtering [52], and hydrothermal process [53, 54]. Notably, the carbon contents in the products from those previous syntheses were all quite low, at a dopant level around 1–3 at.% [50, 52, 54]. In contrast, the 2DA-TCO structure in figure 2(d) is carbon enriched with a composition of 9.1 at.%, possibly making those previous approaches for the synthesis of bulk C-containing titanium oxides less promising. Alternatively, our

Table 1. Elastic constants of the 2DA-101 and 2DA-TCO structures. Unit: GPa.

	C_{11}	C_{12}	C_{22}	C_{66}	Mechanically stable
2DA-101 (TiO_2)	157.4	55.2	150.6	48.3	Yes
2DA-TCO ($Ti_8O_{12}C_2$)	163.2	76.3	197.0	40.4	Yes

recent work [32, 33] may shed light on efficient, large-scale, and cost-effective synthesis of TiO_2-based low-dimensional nanomaterials with high carbon concentrations, thus promising for synthesizing the 2DA-TCO structure discovered in this study. As discussed in the section 1, it was found that 1D titanium carbo-oxides nanofilaments can be synthesized by immersing versatile Ti-containing nonlayered bulk precursors in TMAH aqueous solution at 50 °C or 80 °C for a few days [33]. Nevertheless, we also admit that a lot more research is still needed to further understand the reaction mechanism of this new synthesis approach and to correspondingly design and optimize the synthesis conditions for the 2DA-TCO structure theoretically discovered in this study.

4. Summary

In the present work, first-principles calculations are carried out to study the possible inclusion of C in 2D TiO_2-based structures and the resulting effects on their electronic and elastic properties. An effective structure sampling scheme was implemented to find low energy, dynamically stable forms of 2D TCOs for different C substitutions for O. It is found that an atomic structure close to lepidocrocite TiO_2 is energetically favored when the substitutional content of C is relatively low ($\Delta n_O \leqslant 1/8$). As more O atoms are replaced by C ($1/4 \leqslant n_O \leqslant 1/2$), the energetically favorable structure switches to 2D structures that correspond to the (101) plane facets of anatase TiO_2. At the highest C investigated, viz. $n_O = 1$, the structure relaxes into a configuration with local resemblance to—and the same composition as—O-terminated Ti_2C MXene.

The one-to-one substitution scenario results in the formation of C–C dimers with a quite strong covalent bond between them for which there is scant experimental evidence. Among the searched low energy structures, a structure templating on the (101) plane facet of anatase TiO_2 (i.e. 2DA-TCO) is found to be a possible candidate, wherein two O atoms in the center between the two Ti layers are replaced by one C. It is worth noting here that in that structure the C atoms are bonded to four Ti atoms.

We find that the C-free 2D TiO_2 has a much wider bandgap (~4.3 eV) compared to its bulk counterpart, but that the C-substitution introduce new individual electronic states in the bandgap range. Consequently, the excitation energy from the C state to the conduction band of Ti is reduced to 2.3 eV. The analysis of differential charge density suggests that C-induced states mainly originate from the chemical bonds between Ti and C atoms and the O and C atoms, which show a mixed characteristic of ionic and covalent bonding. The C-substitution is also found to enhance the elastic stiffness of the 2D titanium carbo-oxide, possibly due to the formation of Ti–C bonds.

Lastly, we note that this work is a first step in modeling what we actually experimentally produce: 2D flakes comprised of 1D titanium carbo-oxides nanofilaments [33]. This comment notwithstanding, there is little doubt that the structures that we found are stable and thus possible. We hope this work inspires others to look into synthesizing the novel 2D structures predicted herein.

Data availability statement

All the data and codes related to this study are available upon request from corresponding authors, Y J H (yh593@drexel.edu) and J B (jonas.bjork@liu.se).

Acknowledgments

Y J H, C T, and M W B acknowledge support from the Ceramics Program of the Division of Materials Research of the National Science Foundation (NSF) under award DMR-2211319. Y J H and C T also acknowledge support from the startup fund by Drexel University. M W B also acknowledges support from Murata Corporation of Japan. J R acknowledges support from the Knut and Alice Wallenberg (KAW) Foundation for a Fellowship/Scholar Grant, and from the Göran Gustafsson foundation. Computational resources were partially allocated at the National Supercomputer Centre, Sweden, allocated by SNIC, partially allocated at the Drexel's University Research Computing Facility (Picotte), and partially allocated at Stampede2 at Texas Advanced Computing Center (TACC) through allocation MAT220033 from the Advanced Cyberinfrastructure Coordination Ecosystem: Services & Support (ACCESS) program, which is supported by National Science Foundation Grants #2138259, #2138286, #2138307, #2137603, and #2138296.

ORCID iDs

Yong-Jie Hu https://orcid.org/0000-0003-1500-4015
Jonas Björk https://orcid.org/0000-0002-1345-0006

References

[1] Geim A K 2009 Graphene: status and prospects *Science* **324** 1530–4

[2] Zhang K, Feng Y, Wang F, Yang Z and Wang J 2017 Two dimensional hexagonal boron nitride (2D-hBN): synthesis, properties and applications *J. Mater. Chem.* C **5** 11992–2022

[3] Vogt P, De Padova P, Quaresima C, Avila J, Frantzeskakis E, Asensio M C, Resta A, Ealet B and Le Lay G 2012 Silicene: compelling experimental evidence for graphenelike two-dimensional silicon *Phys. Rev. Lett.* **108** 155501

[4] Acun A, Zhang L, Bampoulis P, Farmanbar M V, van Houselt A, Rudenko A, Lingenfelder M, Brocks G, Poelsema B and Katsnelson M 2015 Germanene: the germanium analogue of graphene *J. Phys.: Condens. Matter* **27** 443002

[5] Kalantar-zadeh K, Ou J Z, Daeneke T, Mitchell A, Sasaki T and Fuhrer M S 2016 Two dimensional and layered transition metal oxides *Appl. Mater. Today* **5** 73–89

[6] Manzeli S, Ovchinnikov D, Pasquier D, Yazyev O V and Kis A 2017 2D transition metal dichalcogenides *J. Nat. Rev. Mater.* **2** 1–15

[7] Naguib M, Kurtoglu M, Presser V, Lu J, Niu J, Heon M, Hultman L, Gogotsi Y and Barsoum M W 2011 Two-dimensional nanocrystals produced by exfoliation of Ti_3AlC_2 *Adv. Mater.* **23** 4248–53

[8] Novoselov K S, Geim A K, Morozov S V, Jiang D-E, Zhang Y, Dubonos S V, Grigorieva I V and Firsov A A 2004 Electric field effect in atomically thin carbon films *science* **306** 666–9

[9] Xia F, Wang H and Jia Y 2014 Rediscovering black phosphorus as an anisotropic layered material for optoelectronics and electronics *Nat. Commun.* **5** 1–6

[10] Verger L, Xu C, Natu V, Cheng H-M, Ren W and Barsoum M W 2019 Overview of the synthesis of MXenes and other ultrathin 2D transition metal carbides and nitrides *Curr. Opin. Solid State Mater. Sci.* **23** 149–63

[11] Swartzen-Allen S L and Matijevic E 1974 Surface and colloid chemistry of clays *Chem. Rev.* **74** 385–400

[12] Cai Z, Liu B, Zou X and Cheng H-M 2018 Chemical vapor deposition growth and applications of two-dimensional materials and their heterostructures *Chem. Rev.* **118** 6091–133

[13] Kim S, Lim H, Lee J and Choi H C 2018 Synthesis of a scalable two-dimensional covalent organic framework by the photon-assisted imine condensation reaction on the water surface *Langmuir* **34** 8731–8

[14] Moreno C *et al* 2018 Bottom-up synthesis of multifunctional nanoporous graphene *Science* **360** 199–203

[15] Grossmann L, King B T, Reichlmaier S, Hartmann N, Rosen J, Heckl W M, Björk J and Lackinger M 2021 On-surface photopolymerization of two-dimensional polymers ordered on the mesoscale *Nat. Chem.* **13** 730–6

[16] Sasaki T, Watanabe M, Michiue Y, Komatsu Y, Izumi F and Takenouchi S 1995 Preparation and acid-base properties of a protonated titanate with the lepidocrocite-like layer structure *Chem. Mater.* **7** 1001–7

[17] Ma J *et al* 2017 Layered lepidocrocite type structure isolated by revisiting the sol–gel chemistry of anatase TiO_2: a new anode material for batteries *Chem. Mater.* **29** 8313–24

[18] Ding D, Liu K, He S, Gao C and Yin Y 2014 Ligand-exchange assisted formation of Au/TiO_2 Schottky contact for visible-light photocatalysis *Nano Lett.* **14** 6731–6

[19] Meng S, Ren J and Kaxiras E 2008 Natural dyes adsorbed on TiO_2 nanowire for photovoltaic applications: enhanced light absorption and ultrafast electron injection *Nano Lett.* **8** 3266–72

[20] Wei Seh Z, Li W, Cha J J, Zheng G, Yang Y, McDowell M T, Hsu P-C and Cui Y 2013 Sulphur–TiO_2 yolk–shell nanoarchitecture with internal void space for long-cycle lithium–sulphur batteries *Nat. Commun.* **4** 1–6

[21] Zhao C, Cai Y, Yin K, Li H, Shen D, Qin N, Lu Z, Liu C and Wang H-E 2018 Carbon-bonded, oxygen-deficient TiO_2 nanotubes with hybridized phases for superior Na-ion storage *Chem.l Eng. J.* **350** 201–8

[22] Zhou W, Umezawa N, Ma R, Sakai N, Ebina Y, Sano K, Liu M, Ishida Y, Aida T and Sasaki T 2018 Spontaneous direct band gap, high hole mobility, and huge exciton energy in atomic-thin TiO_2 nanosheet *Chem. Mater.* **30** 6449–57

[23] Sakai N, Ebina Y, Takada K and Sasaki T 2004 Electronic band structure of titania semiconductor nanosheets revealed by electrochemical and photoelectrochemical studies *J. Am. Chem. Soc.* **126** 5851–8

[24] Sun Z, Liao T, Dou Y, Hwang S M, Park M-S, Jiang L, Kim J H and Dou S X 2014 Generalized self-assembly of scalable two-dimensional transition metal oxide nanosheets *Nat. Commun.* **5** 1–9

[25] Sheng L, Liao T, Kou L and Sun Z 2017 Single-crystalline ultrathin 2D TiO_2 nanosheets: a bridge towards superior photovoltaic devices *Mater. Today Energy* **3** 32–39

[26] Liao T, Sun Z and Dou S X 2017 Theoretically manipulating quantum dots on two-dimensional TiO_2 monolayer for effective visible light absorption *ACS Appl. Mater. Interfaces* **9** 8255–62

[27] Wang S L, Luo X, Zhou X, Zhu Y, Chi X, Chen W, Wu K, Liu Z, Quek S Y and Xu G Q 2017 Fabrication and properties of a free-standing two-dimensional titania *J. Am. Chem. Soc.* **139** 15414–9

[28] Burst J M, Duenow J N, Albin D S, Colegrove E, Reese M O, Aguiar J A, Jiang C S, Patel M K, Al-Jassim M M and Kuciauskas D 2016 CdTe solar cells with open-circuit voltage breaking the 1 V barrier *Nat. Energy* **1** 1–8

[29] Bai Y, Xing Z, Yu H, Li Z, Amal R and Wang L 2013 Porous titania nanosheet/nanoparticle hybrids as photoanodes for dye-sensitized solar cells *ACS Appl. Mater. Interfaces* **5** 12058–65

[30] Li Y, Yin Z, Ji G, Liang Z, Xue Y, Guo Y, Tian J, Wang X and Cui H 2019 2D/2D/2D heterojunction of Ti_3C_2 MXene/MoS_2 nanosheets/TiO_2 nanosheets with exposed (001) facets toward enhanced photocatalytic hydrogen production activity *Appl. Catal.* B **246** 12–20

[31] Chemseddine A and Moritz T 1999 Nanostructuring titania: control over nanocrystal structure, size, shape, and organization *Eur. J. Inorg. Chem.* **1999** 235–45

[32] Badr H O *et al* 2022 Scalable, inexpensive, one pot, synthesis of crystalline two-dimensional birnessite flakes *Matter* **5** 2365–81

[33] Badr H O *et al* 2021 Bottom-up, scalable synthesis of anatase nanofilament-based two-dimensional titanium carbo-oxide flakes *Mater. Today* **54** 8–17

[34] Mai L, Huang C, Wang D, Zhang Z and Wang Y 2009 Effect of C doping on the structural and optical properties of sol–gel TiO_2 thin films *Appl. Surf. Sci.* **255** 9285–9

[35] Yang K, Dai Y, Huang B and Whangbo M-H 2009 Density functional characterization of the visible-light absorption in substitutional C-anion-and C-cation-doped TiO_2 *J. Phys. Chem.* C **113** 2624–9

[36] Kim I, Lee G and Choi M 2020 First-principles investigation of two-dimensional 1 T− TiO_2 *Phys. Rev. Mater.* **4** 094001

[37] Eivari H A, Ghasemi S A, Tahmasbi H, Rostami S, Faraji S, Rasoulkhani R, Goedecker S and Amsler M 2017 Two-dimensional hexagonal sheet of TiO_2 *Chem. Mater.* **29** 8594–603

[38] Kresse G and Furthmüller J 1996 Efficient iterative schemes for *ab initio* total-energy calculations using a plane-wave basis set *Phys. Rev.* B **54** 11169

[39] Blöchl P E 1994 Projector augmented-wave method *Phys. Rev.* B **50** 17953

[40] Perdew J P, Burke K and Ernzerhof M 1996 Generalized gradient approximation made simple *Phys. Rev. Lett.* **77** 3865

[41] Born M, Huang K and Lax M 1955 Dynamical theory of crystal lattices *Am. J. Phys.* **23** 474

[42] Eriksson F, Fransson E and Erhart P 2019 The Hiphive Package for the extraction of high-order force constants by machine learning *Adv. Theory Simul.* **2** 1800184

[43] Heyd J, Scuseria G E and Ernzerhof M 2003 Hybrid functionals based on a screened Coulomb potential *J. Chem. Phys.* **118** 8207–15

[44] Momma K and Izumi F 2011 VESTA 3 for three-dimensional visualization of crystal, volumetric and morphology data *J. Appl. Crystallogr.* **44** 1272–6

[45] Björk J and Rosen J 2021 Functionalizing MXenes by tailoring surface terminations in different chemical environments *Chem. Mater.* **33** 9108–18

[46] Landmann M, Rauls E and Schmidt W G 2012 The electronic structure and optical response of rutile, anatase and brookite TiO_2 *J. Phys.: Condens. Matter* **24** 195503

[47] Nakashima P N H, Smith A E, Etheridge J and Muddle B C 2011 The bonding electron density in aluminum *Science* **331** 1583–6

[48] Hu Y-J, Wang Y, Wang W Y, Darling K A, Kecskes L J and Liu Z-K 2020 Solute effects on the Σ3 111 [11–0] tilt grain boundary in BCC Fe: grain boundary segregation, stability, and embrittlement *Comput. Mater. Sci.* **171** 109271

[49] Mouhat F and Coudert F-X 2014 Necessary and sufficient elastic stability conditions in various crystal systems *Phys. Rev.* B **90** 224104

[50] Wu G, Nishikawa T, Ohtani B and Chen A 2007 Synthesis and characterization of carbon-doped TiO_2 nanostructures with enhanced visible light response *Chem. Mater.* **19** 4530–7

[51] Liu G, Han C, Pelaez M, Zhu D, Liao S, Likodimos V, Ioannidis N, Kontos A G, Falaras P and Dunlop P S M 2012 Synthesis, characterization and photocatalytic evaluation of visible light activated C-doped TiO_2 nanoparticles *Nanotechnology* **23** 294003

[52] Varnagiris S, Medvids A, Lelis M, Milcius D and Antuzevics A 2019 Black carbon-doped TiO_2 films: synthesis, characterization and photocatalysis *J. Photochem. Photobiol.* A **382** 111941

[53] Dong F, Wang H and Wu Z 2009 One-step "green" synthetic approach for mesoporous C-doped titanium dioxide with efficient visible light photocatalytic activity *J. Phys. Chem.* C **113** 16717–23

[54] Yu J, Dai G, Xiang Q and Jaroniec M 2011 Fabrication and enhanced visible-light photocatalytic activity of carbon self-doped TiO_2 sheets with exposed {001} facets *J. Mater. Chem.* **21** 1049–57